

Non-Gaussian superradiant transition via three-body ultrastrong couplingFabrizio Minganti,^{1,2} Louis Garbe,³ Alexandre Le Boité^{4,*} and Simone Felicetti⁵¹*Institute of Physics, Ecole Polytechnique Fédérale de Lausanne, 1015 Lausanne, Switzerland*²*Center for Quantum Science and Engineering, Ecole Polytechnique Fédérale de Lausanne, 1015 Lausanne, Switzerland*³*Vienna Center for Quantum Science and Technology, Atominstytut, TU Wien, 1040 Vienna, Austria*⁴*Laboratoire Matériaux et Phénomènes Quantiques, UMR No. 7162, CNRS, Université Paris Cité, 75013 Paris, France*⁵*Istituto di Fotonica e Nanotecnologie, Consiglio Nazionale delle Ricerche, 00156 Roma, Italy*

(Received 14 April 2022; accepted 23 December 2022; published 20 January 2023)

We introduce a class of quantum optical Hamiltonians characterized by three-body couplings and propose a circuit-QED scheme based on state-of-the-art technology that implements the considered model. Unlike two-body light-matter interactions, this three-body coupling Hamiltonian is exclusively composed of terms which do not conserve the particle number. We explore the three-body ultrastrong-coupling regime, showing the emergence of a superradiant phase transition which is of first order, is characterized by the breaking of $\mathbb{Z}_2 \times \mathbb{Z}_2$ symmetry, and has a strongly non-Gaussian nature. Indeed, in contrast to what is observed in any two-body-coupling model, in proximity of the transition the ground state exhibits a divergent coskewness, i.e., quantum correlations that cannot be captured within semiclassical and Gaussian approximations. Furthermore, we demonstrate the robustness of our findings by including dissipative processes in the model, showing that the steady state of the system inherits from the ground states the most prominent features of the transition.

DOI: [10.1103/PhysRevA.107.013715](https://doi.org/10.1103/PhysRevA.107.013715)**I. INTRODUCTION**

Controlling the interaction between light and matter is one of the main research axes of modern quantum science. It has far-reaching implications for fundamental research and practical applications in quantum optics [1], condensed matter [2,3], and polaritonic chemistry [4,5]. The achievement of the strong-coupling regime, where the interaction strength overcomes losses, led to the observation of quantum-coherent energy exchanges and paved the way to a plethora of applications in quantum technologies. When the coupling strength is further increased, becoming comparable to the bare-system frequencies, the ultrastrong-coupling (USC) regime is reached [6–8], leading to deep modifications of optical, material, and chemical properties.

One of the most debated theoretical predictions regarding the USC regime is the emergence of a superradiant phase transition driven by quantum light-matter interaction [9]. When increasing the coupling strength, the ground-state transitions from the vacuum to a superradiant phase populated by a macroscopic number of photonic excitations. Despite these theoretical predictions, the presence of renormalizing terms in realistic physical settings arguably prevents the emergence of the superradiant phase at equilibrium [10–17]. However, this issue can be circumvented using optical pumping schemes and analog quantum simulation techniques [18], where the light-matter coupling is effectively enhanced and pushed into the USC regime. In the past few years, this approach has been successfully implemented in circuit QED [19–21], trapped ions

[22], opto- and electromechanical devices [23], and atomic systems [24,25]. As a relevant example, analog quantum simulation schemes applied on driven ultracold atoms in an optical cavity led to the observation of superradiant transitions [26–28], where the strength of the light-matter interaction becomes dominant and results in a large number of atomic and photonic excitations in the system steady state.

These effective implementations of USC can reach extreme regimes of parameters, and phase transitions can emerge in systems with a finite number of components [29–32], where the thermodynamic limit is substituted with a rescaling of the parameters. These finite-component phase transitions are easier to control [33] than their many-body counterparts and offer an interesting framework for the study of critical phenomena [34–40]. For instance, it was recently shown [41] that the features of a superradiant phase are universally determined by key spectral properties of the model and thus by the underlying symmetry of the USC interaction. Beyond their fundamental interest, finite-component phase transitions open perspectives for quantum technologies. Notably, finite-component critical phenomena in atomic and solid-state devices are promising candidates for the development of critical quantum sensors [42–53].

Here we introduce a kind of superradiant phase transition, induced by three-body coupling in the USC regime, and propose a scheme to implement this phenomenology based on recent experimental developments [54]. Our model consists of three nonlinear quantum resonators, whose coupling Hamiltonian has $\mathbb{Z}_2 \times \mathbb{Z}_2$ symmetry. We use both analytical and numerical tools to characterize the unconventional properties of its finite-component phase transition. With respect to standard superradiant transitions induced by two-body

*alexandre.leboite@univ-paris-diderot.fr

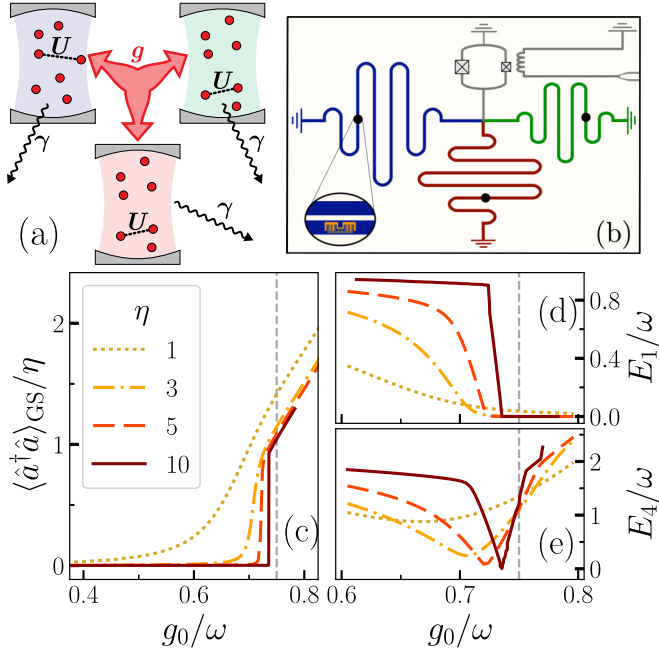


FIG. 1. (a) Schematic representation of a system characterized by three-body USC realized, e.g., by the superconducting circuit in (b). (c) Rescaled photon number $\langle \hat{a}^\dagger \hat{a} \rangle / \eta$ in the ground state [cf. Eq. (2)] vs the three-body coupling strength g_0 . We go towards the thermodynamic limit by increasing η . At the transition, the population shows a discontinuity indicating a first-order transition. Also shown is the energy of (d) the first excited state E_1 and (e) the fourth excited state E_4 . Note that the first three excited states are degenerate, $E_1 = E_2 = E_3$. At the transition, these energies go to zero and we obtain a fourfold-degenerate ground state, signaling spontaneous symmetry breaking. The next excited state E_4 shows the first-order discontinuity. The first-order transition point predicted by the semiclassical theory is indicated by a vertical dashed line in (c)–(e). We set $U_0 / \omega = 1$.

interactions, the most prominent features of our model are (i) the multiple degeneracy of the ground state in the superradiant phase and (ii) the non-Gaussian nature of the ground state at the transition, as certified by the coskewness of the photon statistics. We then present a microwave-pumping scheme that implements the considered model in a circuit-QED device, feasible with current technology. Finally, we provide analytical and numerical evidence that the key features of the phase transition are preserved in the presence of drive and dissipation, showing that this phenomenology is of direct experimental relevance.

II. MODEL

We consider a trimer of nonlinear resonators coupled via a three-body coupling term. Among the different possible designs offered by quantum simulation techniques [see Figs. 1(a) and 1(b)], we focus in this work on the Hamiltonian

$$\begin{aligned} \hat{H} = & \omega \hat{a}^\dagger \hat{a} + \omega \hat{b}^\dagger \hat{b} + \omega \hat{c}^\dagger \hat{c} + U \hat{a}^\dagger \hat{a}^\dagger \hat{a} \hat{a} + U \hat{b}^\dagger \hat{b}^\dagger \hat{b} \hat{b} \\ & + U \hat{c}^\dagger \hat{c}^\dagger \hat{c} \hat{c} + g(\hat{a}^\dagger + \hat{a})(\hat{b}^\dagger + \hat{b})(\hat{c}^\dagger + \hat{c}), \end{aligned} \quad (1)$$

which is a three-body generalization of standard dipolar couplings. We denote by \hat{a} , \hat{b} , and \hat{c} the annihilation operators of three bosonic modes with bare frequencies ω , while U is the on-site nonlinearity and g is the interaction strength. Notice that, if the three resonators have the same frequency, none of the coupling terms in Eq. (1) induces resonant transitions, i.e., all terms are fast oscillating in the interaction picture. However, we find that for three-body interactions the onset of the USC regime, where counterrotating terms become relevant, takes place for very low values of g . We denote by $|\Psi_i\rangle$ and E_i the eigenstates and eigenenergies of the Hamiltonian, respectively, with $E_j \geq E_i$ for $j > i$. Here $i = 0$ corresponds to the ground state. We show in what follows how the superradiant states emerging in the USC regime are strongly constrained by symmetry properties imposed by the specific form of the interaction terms. For the considered model, the Hamiltonian commutes with the operators $\hat{S}_1 = e^{i\pi(\hat{a}^\dagger \hat{a} + \hat{b}^\dagger \hat{b})}$, $\hat{S}_2 = e^{i\pi(\hat{a}^\dagger \hat{a} + \hat{c}^\dagger \hat{c})}$, and $\hat{S}_3 = e^{i\pi(\hat{b}^\dagger \hat{b} + \hat{c}^\dagger \hat{c})}$. Since $\hat{S}_3 = \hat{S}_1 \hat{S}_2$ and $[\hat{S}_1, \hat{S}_2] = 0$, the eigenstates $|\Psi_i\rangle$ are characterized by $\mathbb{Z}_2 \times \mathbb{Z}_2$ symmetry, i.e., two quantum numbers $(s_1, s_2) = (\pm 1, \pm 1)$ such that $\hat{S}_{1,2} |\Psi_i\rangle = s_{1,2} |\Psi_i\rangle$.

III. SUPERRADIANT PHASE TRANSITION

Generally speaking, when the interaction strength g is increased up to values where the coupling term is dominant ($g \gg \omega, U$), a superradiant state always emerges after a crossover [41]. To convert the crossover into a phase transition, an effective thermodynamic limit must be introduced [30,35]. We identify here a parameter-scaling limit that induces a critical transition from the vacuum to a superradiant phase in the considered finite-component setup. This limit consists in letting the nonlinear parameters U and g go to zero while keeping the ratio U/g^2 constant. Formally, this can be done by introducing an effective parameter η and the scaling laws

$$g = \frac{g_0}{\sqrt{\eta}}, \quad U = \frac{U_0}{\eta}, \quad (2)$$

with the thermodynamic limit $\eta \rightarrow \infty$. This choice ensures that all terms in the Hamiltonian scale similarly with η in the superradiant phase, where we expect $\langle \hat{a} \rangle, \langle \hat{b} \rangle, \langle \hat{c} \rangle \sim \sqrt{\eta}$. Let us first investigate the transition at the semiclassical level. We substitute the operators \hat{a} , \hat{b} , and \hat{c} in Eq. (1) with semiclassical fields $\alpha, \beta, \gamma \in \mathbb{C}$ and we look for the energy minima of the resulting potential $H(\alpha, \beta, \gamma)$. Under this approximation the normal-to-superradiant phase transition is driven by the η -independent parameter $\lambda = g\sqrt{2}/\omega U$. We identify three regimes. (i) For $\lambda < 1$, the system is in the normal phase (vacuum). There is no superradiant extremum in $H(\alpha, \beta, \gamma)$. (ii) For $1 < \lambda < 3/(2\sqrt{2})$, $H(\alpha, \beta, \gamma)$ has four superradiant local minima. These states are directly related to the $\mathbb{Z}_2 \times \mathbb{Z}_2$ symmetry. They are obtained by applying the symmetry operators \hat{S}_1 , \hat{S}_2 , and \hat{S}_3 on a coherent state of the form $|\bar{X}, \bar{X}, \bar{X}\rangle$, where $\bar{X} = -\sqrt{\frac{\omega\eta}{2U_0}}(\lambda + \sqrt{\lambda^2 - 1})$. However, the global minimum is still the vacuum. (iii) For $\lambda > 3/(2\sqrt{2})$, the superradiant minima become energetically favorable with respect to the vacuum state and a first-order transition to a superradiant fourfold-degenerate ground state occurs. At this level of

analysis we already see that both the order of the transition and the degeneracy of the ground state are modified with respect to the \mathbb{Z}_2 Dicke-like superradiant transitions. Note that the expected scaling $\langle \hat{a} \rangle, \langle \hat{b} \rangle, \langle \hat{c} \rangle \propto \sqrt{\eta}$ is recovered in the superradiant phase.

We now extend the analytical description including quantum fluctuations via a standard Bogoliubov approach [55]. Namely, we expand the Hamiltonian around the mean-field solutions according to $\hat{a} \rightarrow \bar{X} + \hat{\mu}$, $\hat{b} \rightarrow \bar{X} + \hat{\nu}$, and $\hat{c} \rightarrow \bar{X} + \hat{\zeta}$. Keeping only second-order terms in $\hat{\mu}$, $\hat{\nu}$, and $\hat{\zeta}$ leads to a quadratic Hamiltonian which can be readily diagonalized (see Appendix C). We find that there is a region $\lambda \in]1, 1 + l]$, where $l = (\frac{U_0}{\eta\omega})^{4/5}$, in which fluctuations of the superradiant states are relevant. Thus, the semiclassical picture can be completed as follows. (i) When $1 < \lambda < 1 + l$, quantum fluctuations make the superradiant states unstable. (ii) For $1 + l < \lambda < 3/(2\sqrt{2})$, superradiant local minima are not yet the ground state, but are stable. [Note that in the thermodynamic limit, $l \rightarrow 0$, thus we always have $1 + l < 3/(2\sqrt{2})$.] (iii) For $\lambda > 3/(2\sqrt{2})$, the superradiant states become global minima and the phase transition takes place. This treatment predicts that the fluctuations in both the normal and superradiant states are bounded at the phase transition. This is an important difference with respect to Dicke-like phase transitions, where similar Gaussian treatments predict that the transition is accompanied by large quantum fluctuations.

As presented in Fig. 1, the semiclassical theory correctly predicts some features of the phase transition, as confirmed by exact numerical simulations (see Appendix B). In Fig. 1(c) we show the mean photon number in the ground state as a function of the coupling strength g for different values of η . Even for relatively small η , the results show a discontinuity, a clear signature of a first-order phase transition occurring at $\lambda = 3/(2\sqrt{2})$ (i.e., $g_0/\omega = 0.75$ in Fig. 1). The first-order discontinuity is also revealed by the behavior of the energy of the fourth excited state ($\hat{H}|\Psi_4\rangle = E_4|\Psi_4\rangle$) plotted in Fig. 1(e). The state $|\Psi_4\rangle$ has the same symmetry properties as $|\Psi_{GS}\rangle$ because $\hat{S}_{1,2}|\Psi_4\rangle = |\Psi_4\rangle$ and therefore the avoided level crossing shown in Fig. 1(e) is the precursor of the true criticality [56] emerging in the thermodynamic limit $\eta \rightarrow \infty$. The breaking of the $\mathbb{Z}_2 \times \mathbb{Z}_2$ symmetry is evidenced by the change in the energy spectrum at the transition of $|\Psi_{1,2,3}\rangle$, i.e., the eigenvectors belonging to different symmetry sectors with respect to the ground state. As shown in Fig. 1(d), the energy gap between the ground state and the first three excited states closes and the ground state becomes almost fourfold degenerate for $\lambda \geq 3/(2\sqrt{2})$.

The exact numerical results also reveal a key feature of the transition that is not captured by the semiclassical analysis, namely, its non-Gaussian character. By non-Gaussian we mean that the ground state in the vicinity of the transition cannot be described by any superposition of Gaussian states, as predicted by a mean-field approach, even when quantum corrections are included through Bogoliubov theory. As a witness of non-Gaussianity, we consider the coskewness of modes \hat{a} , \hat{b} , and \hat{c} , defined as

$$C_{abc} = \frac{\langle \hat{x}_a \hat{x}_b \hat{x}_c \rangle}{\sqrt{\langle \hat{x}_a^2 \rangle \langle \hat{x}_b^2 \rangle \langle \hat{x}_c^2 \rangle}}, \quad (3)$$

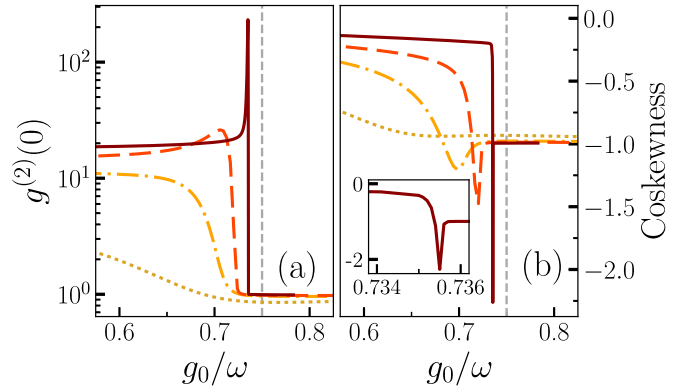


FIG. 2. (a) Rescaled equal-time second-order correlation function $g^{(2)}(0)$ and (b) coskewness of the ground state vs the three-body coupling strength g_0 . The inset shows a close-up of the coskewness for $\eta = 10$. The first-order transition point predicted by the semiclassical theory is indicated by a vertical dashed line. The legend and parameters are the same as in Fig. 1.

where the \hat{x}_i are field quadratures of the form $\hat{x}_a = \hat{a} + \hat{a}^\dagger$. Note that by symmetry, we have $\langle \hat{x}_a \rangle = \langle \hat{x}_b \rangle = \langle \hat{x}_c \rangle = 0$ in $|\Psi_0\rangle$. Mean-field theory predicts that in the superradiant phase $\lim_{\eta \rightarrow \infty} C_{abc} = -1$, while $C_{abc} = 0$ in the normal phase (see Appendix C). Within this approximation, the nonzero value of the coskewness comes from the superposition of coherent states. When quantum fluctuations are included, this quantity remains bounded and we always find $C_{abc} \geq -1$. This stands in sharp contrast to the exact numerical results presented in Fig. 2(b), which exhibit values of the coskewness well below -1 and hint at a divergence at the critical point. To complement the characterization of the ground state, we show in Fig. 2(a) the single-mode second-order correlation function $g^{(2)}(0) = \frac{\langle \hat{a}^\dagger \hat{a}^\dagger \hat{a} \hat{a} \rangle}{\langle \hat{a}^\dagger \hat{a} \rangle^2}$, as a function of the coupling strength. In terms of photon statistics the ground state undergoes a super-Poissonian-to-Poissonian transition, which does not reveal any non-Gaussian behavior such as photon antibunching. It is thus only when considering three-mode correlation functions, such as the coskewness, that the non-Gaussian nature of this superradiant transition becomes apparent.

IV. IMPLEMENTATION WITH SUPERCONDUCTING CIRCUITS

Let us now present a scheme to observe this rich phenomenology with current circuit-QED devices [57,58]. We generalize the scheme proposed in [59] and experimentally implemented in [21], which makes use of a spontaneous parametric down-conversion (SPDC) to induce an effective USC coupling between two microwave resonators. Here we consider instead a three-photon SPDC process where a single (pump) photon is down-converted in a photon triplet. This quantum process has been recently implemented [54] using a superconducting transmission-line resonator grounded through an asymmetric fluxed-pumped superconducting quantum interference device (SQUID). Non-Gaussian state generation has also been demonstrated [60,61]. The model of Eq. (1) can be implemented using the three-resonator scheme sketched in Fig. 1(b). Note that even if similar results

might be obtained with a single multimode resonator, a multi-resonator scheme allows for an independent control of the local Kerr nonlinearities. The circuit scheme here presented is meant to show that it is physically possible to implement the considered model, but a detailed engineering would still be required to design an optimal experimental implementation. The relevant terms in the SQUID Hamiltonian that generate the required nonlinear processes can be written as [54]

$$\hat{H}_{\text{SQ}} = \beta_d(t) \sum \chi_k (\hat{a}^\dagger + \hat{a} + \hat{b}^\dagger + \hat{b} + \hat{c}^\dagger + \hat{c})^k, \quad (4)$$

where \hat{a} , \hat{b} , and \hat{c} are high-quality-factor microwave modes. The cubic terms ($k=3$) responsible for the three-photon parametric processes are nonvanishing for an asymmetric flux-driven SQUID. Most importantly, they can be selectively and simultaneously activated by carefully choosing the drive frequencies (see Appendix A). In our scheme, we take the pump to be composed of four harmonic components $\beta_d(t) = \beta_d \sum_i \cos(\omega_i t)$, each of them inducing a third-order parametric interaction. The corresponding Hamiltonian terms can be written as

$$\begin{aligned} \omega_1 = |\omega_a + \omega_b + \omega_c + \Delta_1| &\rightarrow \hat{H}_1 = \hat{a}^\dagger \hat{b}^\dagger \hat{c}^\dagger + \text{H.c.}, \\ \omega_2 = |\omega_a + \omega_b - \omega_c + \Delta_2| &\rightarrow \hat{H}_2 = \hat{a}^\dagger \hat{b}^\dagger \hat{c} + \text{H.c.}, \\ \omega_3 = |\omega_a - \omega_b + \omega_c + \Delta_3| &\rightarrow \hat{H}_3 = \hat{a}^\dagger \hat{b} \hat{c}^\dagger + \text{H.c.}, \\ \omega_4 = |\omega_a - \omega_b - \omega_c + \Delta_4| &\rightarrow \hat{H}_4 = \hat{a}^\dagger \hat{b} \hat{c} + \text{H.c.}, \end{aligned} \quad (5)$$

where ω_a , ω_b , and ω_c are the characteristic frequencies of the resonators, while Δ_i are small detunings. The sum of the four contributions \hat{H}_i reproduces the three-body-interaction term

$$\hat{H}_{\text{SQ}} \approx g \sum_i \hat{H}_i = g(\hat{a}^\dagger + \hat{a})(\hat{b}^\dagger + \hat{b})(\hat{c}^\dagger + \hat{c}), \quad (6)$$

where the pump-induced coupling is given by $g = \beta_d \chi_3/2$. The small detunings $\Delta_i \ll \omega_i$ will establish the frequencies of the bare modes in the effective Hamiltonian, which are resonant for $\Delta_1 = 3\omega$ and $\Delta_2 = \Delta_3 = \Delta_4 = \omega$. The full target model of Eq. (1) is then reproduced in the interaction picture with respect to the Hamiltonian $H_0 = (\omega_a - \omega)\hat{a}^\dagger \hat{a} + (\omega_b - \omega)\hat{b}^\dagger \hat{b} + (\omega_c - \omega)\hat{c}^\dagger \hat{c}$. Intrinsic Kerr and cross-Kerr terms are present due to the nonlinearity of the SQUID. However, engineering a local nonlinear element, such as weakly coupled qubits [57,58], allows one to make individual Kerr terms dominant and to tune the size of the nonlinearity. Note that the unavoidable presence of cross-Kerr terms is not an intrinsic limitation and it might even result in a richer phase diagram. Given that the present work represents a proof-of-concept study of ultrastrong three-body couplings, we have decided to consider a minimal Hamiltonian in order to identify the specific properties of this class of interaction. However, for an actual experimental realization, it might be favorable to consider generalizations of the model of Eq. (1) which have a similar phenomenology but are less challenging to implement. On the other hand, real-time tuning of the nonlinearity is of high relevance, as it makes it possible to explore the finite-frequency scaling with a single sample, although the mode frequencies must be carefully chosen in order to prevent the activation of spurious interaction terms (see Appendix A). Unwanted couplings can become relevant when one of the pump frequencies is close to two-body resonances $\omega_i \approx \omega_a \pm \omega_b$ or

if parametric processes involving nonfundamental modes of the resonators are activated (for instance, $\omega_i \approx \omega_a \pm \omega_b \pm \omega_d$, with ω_d the frequency of any higher-order resonator mode).

V. DRIVEN-DISSIPATIVE PHASE TRANSITION

Like any quantum optical setup, the proposed implementation is subject to unavoidable dissipative processes [62]. In this dissipative context, a phase transition occurs in the steady state, which is reached in the long-time limit under the competition between the unitary dynamics and the loss mechanisms [63,64]. We model the driven-dissipative dynamics by the Lindblad master equation

$$\begin{aligned} \frac{d}{dt} \hat{\rho}(t) = \mathcal{L} \hat{\rho}(t) = & -i[\hat{H}, \hat{\rho}(t)] + \kappa \mathcal{D}[\hat{a}] \hat{\rho}(t) \\ & + \kappa \mathcal{D}[\hat{b}] \hat{\rho}(t) + \kappa \mathcal{D}[\hat{c}] \hat{\rho}(t), \end{aligned} \quad (7)$$

where $\hat{\rho}(t)$ denotes the density matrix of the system. The dissipators describing single-photon losses are defined as $\mathcal{D}[\hat{O}] \hat{\rho}(t) = \hat{O} \hat{\rho}(t) \hat{O}^\dagger - [\hat{O}^\dagger \hat{O} \hat{\rho}(t) + \hat{\rho}(t) \hat{O}^\dagger \hat{O}]/2$ and occur at a rate κ . Note that in this effective implementation of the USC regime, single-photon losses do not trivially drive the system towards the ground state of the Hamiltonian \hat{H} . Besides unavoidable single-photon losses, the drive can mediate higher-order [65] three-photon dissipative processes. These processes, however, are subdominant in the parameter regime we consider and can be safely neglected [54]. Within the density-matrix formalism, the symmetry operators \hat{S}_i are extended to the superoperator level by $\mathcal{S}_i \hat{\rho} = \hat{S}_i \hat{\rho} \hat{S}_i^\dagger$ [66–68]. In the present case, the Liouvillian \mathcal{L} has the same symmetry as \hat{H} , namely,

$$[\mathcal{S}_i, \mathcal{L}] = 0. \quad (8)$$

Hence the results of the symmetry analysis extend from the ground state to the steady state.

We simulate the dynamics in Eq. (8) using a quantum trajectory approach, where the resulting density matrix is obtained by averaging over a large number of realizations of a stochastic Schrödinger equation (see Appendix B). The steady-state values are then obtained by evolving the results for sufficiently long times. The number of realizations is chosen large enough to ensure that the uncertainty on the value of the observables is smaller than 5%. Three factors make the simulation demanding for large- η values: (i) Growing photon numbers require a large cutoff, (ii) the non-Gaussian nature of the state implies long tails in the photon-number distribution, and (iii) the state is extremely entropic at the phase transition, requiring a large trajectory sample to obtain non-noisy data. In Fig. 3(a) we show the average photon number as a function of the coupling g , for a dissipation rate equal to the bare frequency $\kappa = \omega$. Similarly to the nondissipative case, we observe a sharper change in the photon number as the parameter η increases. Notice also that the transition point is slightly shifted with respect to the nondissipative case. Finally, in Fig. 3(b) we show that also in the dissipative case the coskewness drops below -1 , signaling the non-Gaussian nature of the transition, even for a rather high dissipation rate. We thus confirm that the proposed implementation allows

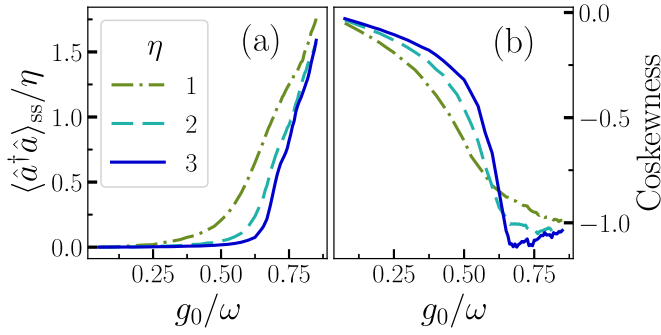


FIG. 3. (a) Rescaled photon number and (b) coskewness of the steady state vs the three-body coupling strength g_0 . The parameters are the same as in Fig. 1 and $\kappa = \omega$. The number of trajectories at each point ensures that observables reached convergence within an error of 5%. Even for these values of noise, we still achieve a coskewness below -1 .

witnessing the unconventional properties of superradiant phase transitions induced by ultrastrong three-body coupling.

VI. CONCLUSION

We have demonstrated that a trimer of nonlinear oscillators coupled via a three-body terms exhibits a superradiant phase transition in the USC regime. In contrast with the usual two-body dipolar coupling, the three-body Hamiltonian leads to large non-Gaussian quantum fluctuations, as witnessed by a diverging coskewness in the vicinity of the transition. Exact numerical simulations show that these features, which are captured neither by semiclassical analysis nor by the Bogoliubov approach, are robust to dissipation and could be observed with the proposed circuit-QED scheme. Our results demonstrate the theoretical and experimental relevance of three-body couplings in open quantum-optical systems. This work introduces the study of ultrastrong three-body couplings and it is focused on static properties, in both the Hamiltonian and the dissipative settings. Further analyses of this class of models can lead to the observation of a richer quantum phenomenology related to the ultrastrong-coupling regime [6–8]. For example, investigations of dynamical properties across the transition in closed or open settings offer interesting perspectives [69]. Beyond the intrinsic interest in an unconventional quantum phenomenology, three-body interactions can be used in the generation of quantum non-Gaussian states [70–73], in quantum sensing [47] applications, and in quantum-information processing [74].

ACKNOWLEDGMENTS

We thank M. Genoni for interesting discussions. A.L.B. and S.F. acknowledge support from CNRS via the International Emerging Action project DDMolPol (Project No. 203844). L.G. was supported by the Austrian Academy of Sciences (ÖAW) and by the Austrian Science Fund (FWF) through Grant No. M3214 (ASYMM-LM).

APPENDIX A: EFFECTIVE IMPLEMENTATION

Let us now provide more details on the proposed effective implementation that can reproduce the desired model. In

particular, we will discuss the requirements that the driving fields and the resonator mode structure must fulfill in order to avoid the activation of unwanted coupling terms. The full quantum model for the three-resonator setup sketched in Fig. 1(b) can be written as

$$\hat{H} = \sum_n \{ \omega_a^{(n)} \hat{a}_n^\dagger \hat{a}_n + \omega_b^{(n)} \hat{b}_n^\dagger \hat{b}_n + \omega_c^{(n)} \hat{c}_n^\dagger \hat{c}_n \} + \hat{H}_{\text{Kerr}} + \hat{H}_{\text{SQ}}, \quad (\text{A1})$$

where

$$\hat{H}_{\text{Kerr}} = \sum_n U^{(n)} (\hat{a}_n^{\dagger 2} \hat{a}_n^2 + \hat{b}_n^{\dagger 2} \hat{b}_n^2 + \hat{c}_n^{\dagger 2} \hat{c}_n^2). \quad (\text{A2})$$

We defined the modes \hat{a}_n of the resonator a , with resonant frequency $\omega_a^{(n)}$ and Kerr strength $U^{(n)}$, and similarly for the resonators b and c . Note that $n=0$ corresponds to the fundamental mode considered in the main text $\hat{a}_0 \equiv \hat{a}$, where we dropped the suffix for the sake of simplicity. The full SQUID Hamiltonian then reads

$$\hat{H}_{\text{SQ}} = \Sigma_d \sum_k \chi_k \left[\sum_n (\hat{a}_n^\dagger + \hat{a}_n + \hat{b}_n^\dagger + \hat{b}_n + \hat{c}_n^\dagger + \hat{c}_n) \right]^k, \quad (\text{A3})$$

where $\Sigma_d = \beta_d [\sum_i \cos(\omega_i t)]$. In the interaction picture defined by the harmonic part of the free Hamiltonian, the annihilation and creation operators each rotate at the corresponding resonant frequency $\hat{a}_n(t) = \hat{a}_n e^{i\omega_a^{(n)} t}$ and fast oscillating terms can be neglected by rotating-wave approximation given that $\beta_d \chi_k$ is much smaller than all mode frequencies. As a first condition, we take the three resonators to have different fundamental frequencies $\omega_a^{(0)} \neq \omega_b^{(0)} \neq \omega_c^{(0)}$ in such a way that intrinsic coupling terms are off-resonant and so photon transfer is possible only when mediated by the drivings. We then have to select the frequencies ω_i of the harmonic components of the driving field in such a way that the desired processes are resonant and no spurious terms are activated. In order to reproduce the three-photon coupling we need four components

$$\begin{aligned} \omega_1 &= |\omega_a^{(0)} + \omega_b^{(0)} + \omega_c^{(0)} + \Delta_1|, \\ \omega_2 &= |\omega_a^{(0)} + \omega_b^{(0)} - \omega_c^{(0)} + \Delta_2|, \\ \omega_3 &= |\omega_a^{(0)} - \omega_b^{(0)} + \omega_c^{(0)} + \Delta_3|, \\ \omega_4 &= |\omega_a^{(0)} - \omega_b^{(0)} - \omega_c^{(0)} + \Delta_4|. \end{aligned} \quad (\text{A4})$$

Each of these driving tones will selectively activate an interaction term

$$\begin{aligned} \hat{H}_1 &= \frac{\beta_d \chi_3}{2} (\hat{a}_0^\dagger \hat{b}_0^\dagger \hat{c}_0^\dagger + \text{H.c.}), \\ \hat{H}_2 &= \frac{\beta_d \chi_3}{2} (\hat{a}_0^\dagger \hat{b}_0^\dagger \hat{c}_0 + \text{H.c.}), \\ \hat{H}_3 &= \frac{\beta_d \chi_3}{2} (\hat{a}_0^\dagger \hat{b}_0 \hat{c}_0^\dagger + \text{H.c.}), \\ \hat{H}_4 &= \frac{\beta_d \chi_3}{2} (\hat{a}_0 \hat{b}_0^\dagger \hat{c}_0^\dagger + \text{H.c.}). \end{aligned} \quad (\text{A5})$$

As explained in the main text, the small detunings $\Delta_i \ll \omega_i$ will establish the frequency ω of the bare modes in the effective Hamiltonian $\Delta_1 = 3\omega$ and $\Delta_2 = \Delta_3 = \Delta_4 = \omega$.

Furthermore, the driving frequencies must be significantly detuned from all resonances that induce energy transfer or parametric couplings between fundamental and higher modes. In particular, two kinds of unwanted terms might be activated: two-photon processes such as $\hat{a}_0\hat{b}_1^\dagger$, non-negligible for some $\omega_i \sim \omega_b^{(1)} - \omega_a^{(0)}$, and three-photon processes such as $\hat{a}_0^\dagger\hat{c}_1^\dagger\hat{c}_1^\dagger$, which can be activated when $\omega_i \sim 2\omega_c^{(1)} + \omega_a^{(0)}$. In order for these processes to be negligible, all driving frequencies ω_i must be detuned by an amount δ which is large with respect to the effective coupling strength.

For a given choice of mode frequencies, we can numerically check the detuning with respect to all undesired resonances. Let us provide an example of a suitable set of parameters which is in line with the experimental implementation presented in [54]: $(\omega_a^{(0)}, \omega_b^{(0)}, \omega_c^{(0)}) = 2\pi(7.6, 6.2, 4.2)$ GHz and $(\omega_a^{(1)}, \omega_b^{(1)}, \omega_c^{(1)}) = 2\pi(11.4, 9.3, 6.3)$ GHz. For this set of frequencies and choosing the drive tones as in Eq. (A4), we find that the closest unwanted resonance is given by $\delta = \omega_1 - \omega_a^{(0)} - \omega_c^{(0)} - \omega_c^{(1)} = 2\pi \cdot 0.1$ GHz and other three-photon processes with the same detuning δ . We have to compare this detuning with the strength $g = \frac{\beta_d \chi_3}{2}$ of the process which, in order to observe the transition described in the main text, must reach a value such that $\lambda = \sqrt{2/\omega U}g = 3/(2\sqrt{2})$ and so $g = 3\sqrt{\omega U}/4$. If we set now the frequency of the effective model $\omega = 2\pi \cdot 10$ MHz and $U = \omega/10$ (corresponding to $\eta = 10$), we have that $g \sim 2\pi \cdot 2.4$. Accordingly, the ratio $g/\delta \sim 2.4^{-2}$ is much smaller than 1 and these processes are safely negligible with standard physical parameters [21,54].

APPENDIX B: NUMERICAL SIMULATIONS

1. Hamiltonian numerical simulations

To resolve the spectral features of the Hamiltonian model, we resort to exact diagonalization. This means that we set a cutoff C such that, for any $m > C$ or $n > C$, $\langle m_j | \hat{H} | n_j \rangle = 0$, where $|m_j\rangle$ and $|n_j\rangle$ represent Fock states with m or n photons in the j th cavity. To verify the convergence of our results, we compare the results obtained for a cutoff C and those obtained for a cutoff $C' = C + \eta + 2$. In particular, we verify that the eigenvectors $|\Psi_j(C)\rangle$ associated with the ten lowest eigenenergies E_j and obtained with a cutoff C are less than 0.5% different with respect to those obtained with a cutoff C' , i.e.,

$$|\langle \Psi_j(C) | \Psi_j(C') \rangle| < 0.005. \quad (\text{B1})$$

In the exact diagonalization algorithm, we exploit both the $\mathbb{Z}_2 \times \mathbb{Z}_2$ symmetry of \hat{H} and the translational invariance of the Hamiltonian, to transform \hat{H} into its block-diagonal form. We then diagonalize each one of the blocks, obtaining the eigenvalues and eigenvectors associated with each one of these symmetry sectors. Note that this procedure allows us to determine the correct form of the ground and excited states even in regimes where numerical errors would make it impossible to distinguish between them. Indeed, from analytical considerations, we know that, for any finite-size system, phase transitions cannot occur without a thermodynamical or parameter rescaling limit. Therefore, the eigenvalues of the Hamiltonian can never become truly degenerate.

2. Dissipative numerical simulations

To investigate the dissipative model, we resort to quantum trajectories. A quantum trajectory (also known as wavefunction Monte Carlo) is a mapping of the Lindblad master equation onto a stochastic differential equation for the wave function $|\psi(t)\rangle$. The wave function $|\psi(t)\rangle$ has a piecewise deterministic evolution under the action of a non-Hermitian Hamiltonian \hat{H}_{eff} , which in our case reads

$$\hat{H}_{\text{eff}} = \hat{H} - i\frac{\gamma}{2}(\hat{a}^\dagger\hat{a} + \hat{b}^\dagger\hat{b} + \hat{c}^\dagger\hat{c}), \quad (\text{B2})$$

randomly interrupted by the occurrence of quantum jumps \hat{J} (one of the three operators \hat{a} , \hat{b} , or \hat{c}). In an infinitesimal time step dt , each quantum jump occurs with a probability $p_J = \gamma dt \langle \hat{J}^\dagger \hat{J} \rangle$, where $\hat{J} \in \{\hat{a}, \hat{b}, \hat{c}\}$.

A numerical simulation of a quantum trajectory is thus equivalent to extract the probability that a quantum jump occurred at each time step dt . If no quantum jump occurs, then

$$|\psi(t+dt)\rangle = |\psi(t)\rangle - idt\hat{H}_{\text{eff}}|\psi(t)\rangle. \quad (\text{B3})$$

Otherwise, according to the quantum jump extracted, the evolution is given by

$$|\psi(t+dt)\rangle = \frac{\hat{J}|\psi(t)\rangle}{\langle \psi(t) | \hat{J}^\dagger \hat{J} | \psi(t) \rangle}. \quad (\text{B4})$$

The results of the Lindblad master equation can then be retrieved by averaging over a large number N_{traj} of quantum trajectories, because

$$\hat{\rho}(t) = \lim_{N_{\text{traj}} \rightarrow \infty} \sum_{j=1}^{N_{\text{traj}}} \frac{|\Psi_j(t)\rangle \langle \Psi_j(t)|}{N_{\text{traj}}}. \quad (\text{B5})$$

The advantage of quantum trajectories is thus to reduce the numerical cost of a single simulation (from that of a density matrix to one of a wave function), but the price to pay is the need to perform the simulation several times. To obtain the results shown in the main text, we exploited the parallelizable nature of quantum trajectories. Note that for the largest η considered here, i.e., $\eta = 3$, we were able to obtain reliable results only when considering a cutoff $C = 25$ ($C' = 30$) and thus a Hilbert space of dimension 15 625 (27 000). This demonstrates the very non-Gaussian photon-number distribution of the states across the transition. Furthermore, at the transition, phenomena such as hysteresis require (i) long simulations and (ii) increased mixed nature of the steady state, making it necessary to increase the number of quantum trajectories to reduce the statistical noise.

APPENDIX C: SEMICLASSICAL TREATMENT

1. Mean-field approximation

We will first study the trimer Hamiltonian of Eq. (1) with a mean-field approach, i.e., we assume that each field can be put in a coherent state: $\hat{a} \rightarrow \alpha$, $\hat{b} \rightarrow \beta$, and $\hat{c} \rightarrow \gamma$; the consistency of this hypothesis will be studied at the end of this section. The Hamiltonian then reduces to a classical

potential

$$H(\alpha, \beta, \gamma) = \omega(|\alpha|^2 + |\beta|^2 + |\gamma|^2) + \frac{g_0}{\sqrt{\eta}}(\alpha + \alpha^*)(\beta + \beta^*)(\gamma + \gamma^*) + \frac{U_0}{\eta}(|\alpha|^4 + |\beta|^4 + |\gamma|^4). \quad (\text{C1})$$

The goal then is to find the minima and maxima of this function, which satisfy $\partial H/\partial\alpha = \partial H/\partial\beta = \partial H/\partial\gamma = 0$. We find nine solutions $\alpha = \beta = \gamma = 0$, $\alpha = \beta = -\gamma = X_{\pm}$, $\alpha = -\beta = \gamma = X_{\pm}$, $-\alpha = \beta = \gamma = X_{\pm}$, and $\alpha = \beta = \gamma = -X_{\pm}$, with

$$X_{\pm} = \sqrt{\frac{\omega\eta}{2U_0}}(\lambda \pm \sqrt{\lambda^2 - 1}) = \sqrt{\frac{\omega\eta}{2U_0}}f_{\pm}(\lambda), \quad (\text{C2})$$

where we have defined

$$\lambda = \sqrt{\frac{2}{\omega U_0}}g_0 = \sqrt{\frac{2}{\omega U}}g. \quad (\text{C3})$$

Note that these solutions exist only for $\lambda > 1$. The eight solutions can be grouped into two sets of four degenerate solutions, with a (semiclassical) energy

$$E_{\pm}(\lambda) = \frac{3\omega^2\eta}{4U_0} \left(2f_{\pm}(\lambda)^2 - \frac{8}{3}\lambda f_{\pm}(\lambda)^3 + f_{\pm}(\lambda)^4 \right). \quad (\text{C4})$$

Importantly, we have $E_- \geq 0$ and $E_- \geq E_+$. To summarize, for $\lambda < 1$, we have a semiclassical potential with a single minimum which corresponds to the vacuum. For $\lambda > 1$, the potential has five asymmetric minima and four maxima. The five minima correspond to the vacuum and the four solutions X_+ and have energy $E = 0$ and $E = E_+$, respectively. The maxima correspond to the four solutions X_- , with an energy $E = E_-$. With this analysis, we can already predict that the solutions X_+ will always be unstable.

To better visualize the structure of the potential, let us see what happens if we move along the line $\alpha = \beta = \gamma$. Starting from $\alpha = 0$, the potential increases until we reach $\alpha = X_-$; it then decreases until $\alpha = X_+$ and then goes up again. We obtain the same picture if we follow the line $\alpha = \beta = -\gamma$ and so on. At first, for λ above 1, the four superradiant states can then exist as metastable states, existing in wells of typical width $X_+ - X_-$ and with a potential barrier of height $|E_+ - E_-|$. As λ increases, the depth of the four wells increases. It is straightforward to show that, at $\lambda = \frac{3}{2\sqrt{2}}$, E_+ becomes smaller than the vacuum energy 0. At this point, the four superradiant solutions become the new (degenerate) ground state and a first-order phase transition takes place. In the following, to simplify notation, we will rewrite the position of the local minima as $\bar{X} = -X_-$; this is the notation we used in the main text.

2. Quantum fluctuations

The treatment above predicts that superradiant states become energetically favored above a certain threshold for the coupling. However, quantum fluctuations can also induce tunneling between different states and change their stability. We will now estimate the importance of these fluctuations by a quadratic expansion around the semiclassical solution.

a. Quadratic expansion and Bogoliubov transformation

Let us consider the phase corresponding to $\alpha = \beta = \gamma = \bar{X}$ (the other three phases will have the same stability, by symmetry). We can then decompose the bosonic field into its mean-field value plus quantum fluctuations:

$$\hat{a} \rightarrow \bar{X} + \hat{\mu}, \quad \hat{b} \rightarrow \bar{X} + \hat{\nu}, \quad \hat{c} \rightarrow \bar{X} + \hat{\zeta}.$$

We can then develop the Hamiltonian in various orders of perturbation. The zeroth-order term is a constant and corresponds to the semiclassical energy E_+ . The first-order term is zero, since we are developing around an energy extremum. The second-order term is

$$\begin{aligned} \hat{H}^{(2)} = & \frac{\omega}{4}[1 + f_+(\lambda)^2](\hat{p}_{\mu}^2 + \hat{p}_{\nu}^2 + \hat{p}_{\zeta}^2) \\ & + \frac{\omega}{4}[1 + 3f_+(\lambda)^2](\hat{x}_{\mu}^2 + \hat{x}_{\nu}^2 + \hat{x}_{\zeta}^2) \\ & - \omega\lambda f_+(\lambda)(\hat{x}_{\mu}\hat{x}_{\nu} + \hat{x}_{\nu}\hat{x}_{\zeta} + \hat{x}_{\zeta}\hat{x}_{\mu}), \end{aligned} \quad (\text{C5})$$

where we have defined the quadratures $\hat{x}_{\mu} = \hat{\mu} + \hat{\mu}^{\dagger}$ and so on. This Hamiltonian can be diagonalized with a Bogoliubov transformation. We define new fields \hat{u} , \hat{y} , and \hat{z} as

$$\begin{bmatrix} \hat{x}_{\mu} \\ \hat{x}_{\nu} \\ \hat{x}_{\zeta} \end{bmatrix} = \frac{1}{\sqrt{3}} \begin{pmatrix} 1 + f_+^2 \\ 1 + 3f_+^2 \end{pmatrix}^{1/4} \begin{bmatrix} 1 & 1 & 1 \\ -\frac{1+\sqrt{3}}{2} & 1 & \frac{\sqrt{3}-1}{2} \\ \frac{\sqrt{3}-1}{2} & 1 & -\frac{1+\sqrt{3}}{2} \end{bmatrix} \begin{bmatrix} \hat{u} \\ \hat{y} \\ \hat{z} \end{bmatrix}. \quad (\text{C6})$$

The conjugate variables \hat{p}_u , \hat{p}_y , and \hat{p}_z are instead defined by

$$\begin{bmatrix} \hat{p}_{\mu} \\ \hat{p}_{\nu} \\ \hat{p}_{\zeta} \end{bmatrix} = \frac{1}{\sqrt{3}} \begin{pmatrix} 1 + 3f_+^2 \\ 1 + f_+^2 \end{pmatrix}^{1/4} \begin{bmatrix} 1 & 1 & 1 \\ -\frac{1+\sqrt{3}}{2} & 1 & \frac{\sqrt{3}-1}{2} \\ \frac{\sqrt{3}-1}{2} & 1 & -\frac{1+\sqrt{3}}{2} \end{bmatrix} \begin{bmatrix} \hat{p}_u \\ \hat{p}_y \\ \hat{p}_z \end{bmatrix}. \quad (\text{C7})$$

These operators define collective excitations of the three resonators. In terms of these new degrees of freedom, the Hamiltonian above reads

$$\begin{aligned} \hat{H}^{(2)} = & \frac{\tilde{\omega}}{4}(\hat{p}_u^2 + \hat{p}_y^2 + \hat{p}_z^2) \\ & + \frac{\tilde{\omega}}{4} \left[\hat{u}^2 \left(1 + \frac{\tilde{\lambda}}{2} \right) + \hat{z}^2 \left(1 + \frac{\tilde{\lambda}}{2} \right) + \hat{y}^2 (1 - \tilde{\lambda}) \right], \end{aligned} \quad (\text{C8})$$

where the renormalized coupling $\tilde{\lambda}$ and frequency $\tilde{\omega}$ are defined as

$$1 - \tilde{\lambda} = \sqrt{\lambda^2 - 1} \left(\frac{\lambda + \sqrt{\lambda^2 - 1}}{3\lambda\sqrt{\lambda^2 - 1} + 3\lambda^2 - 1} \right), \quad \tilde{\omega} = \omega\sqrt{(1 + f_+^2)(1 + 3f_+^2)}. \quad (\text{C9})$$

One can readily check that, for $\lambda > 1$, all collective modes are stable and have bounded fluctuations. At $\lambda = \tilde{\lambda} = 1$, however, the y polariton becomes unstable. This is compatible with the mean-field treatment, which predicted that superradiant states exist only for $\lambda > 1$ in the first place.

b. Analysis of fluctuations

Let us study in detail the quadrature fluctuations predicted by the previous analysis. In the normal phase, we have the

usual vacuum fluctuations $\langle \hat{x}_i^2 \rangle = \langle \hat{p}_i^2 \rangle = 1$ and $\langle \hat{x}_i \hat{x}_j \rangle = 0$ for $i = \mu, \nu, \zeta$. In the superradiant phase, combining Eqs. (C6) and (C8), we find the values $\langle \hat{p}_y^2 \rangle = \sqrt{1 - \tilde{\lambda}}$ and $\langle \hat{u} \hat{y} \rangle = \langle \hat{z} \hat{y} \rangle = \langle \hat{u} \hat{z} \rangle = \langle \hat{p}_u \hat{p}_y \rangle = \langle \hat{p}_z \hat{p}_y \rangle = \langle \hat{p}_u \hat{p}_z \rangle = 0$. With this, we find the expressions for the fluctuations of the u , y , and z quadratures

$$\langle \hat{u}^2 \rangle = \langle \hat{z}^2 \rangle = \frac{1}{\sqrt{1 + \tilde{\lambda}/2}}, \quad (\text{C10})$$

$$\langle \hat{y}^2 \rangle = \frac{1}{\sqrt{1 - \tilde{\lambda}}}, \quad (\text{C11})$$

$$\langle \hat{u} \hat{y} \rangle = \langle \hat{z} \hat{y} \rangle = \langle \hat{u} \hat{z} \rangle = 0, \quad (\text{C12})$$

$$\langle \hat{x}_\mu^2 \rangle = \langle \hat{x}_\nu^2 \rangle = \langle \hat{x}_\zeta^2 \rangle = \frac{1}{3} \left(\frac{1 + f_+^2}{1 + 3f_+^2} \right)^{1/2} (2\langle \hat{z}^2 \rangle + \langle \hat{y}^2 \rangle), \quad (\text{C13})$$

$$\langle \hat{x}_\mu \hat{x}_\nu \rangle = \langle \hat{x}_\nu \hat{x}_\zeta \rangle = \langle \hat{x}_\zeta \hat{x}_\mu \rangle = \frac{1}{3} \left(\frac{1 + f_+^2}{1 + 3f_+^2} \right)^{1/2} (\langle \hat{y}^2 \rangle - \langle \hat{z}^2 \rangle), \quad (\text{C14})$$

$$\langle \hat{x}_\mu \hat{x}_\nu \hat{x}_\zeta \rangle = 0, \quad (\text{C15})$$

and for the p quadratures

$$\langle \hat{p}_u^2 \rangle = \langle \hat{p}_z^2 \rangle = \sqrt{1 + \tilde{\lambda}/2}, \quad (\text{C16})$$

$$\langle \hat{p}_y^2 \rangle = \sqrt{1 - \tilde{\lambda}}, \quad (\text{C17})$$

$$\langle \hat{p}_z \hat{p}_y \rangle = \langle \hat{p}_u \hat{p}_z \rangle = \langle \hat{p}_u \hat{p}_y \rangle = 0, \quad (\text{C18})$$

$$\langle \hat{p}_\mu^2 \rangle = \langle \hat{p}_\nu^2 \rangle = \langle \hat{p}_\zeta^2 \rangle = \frac{1}{3} \left(\frac{1 + 3f_+^2}{1 + f_+^2} \right)^{1/2} (2\langle \hat{p}_z^2 \rangle + \langle \hat{p}_y^2 \rangle), \quad (\text{C19})$$

$$\begin{aligned} \langle \hat{p}_\mu \hat{p}_\nu \rangle &= \langle \hat{p}_\nu \hat{p}_\zeta \rangle = \langle \hat{p}_\zeta \hat{p}_\mu \rangle \\ &= \frac{1}{3} \left(\frac{1 + 3f_+^2}{1 + f_+^2} \right)^{1/2} (\langle \hat{p}_y^2 \rangle - \langle \hat{p}_z^2 \rangle), \end{aligned} \quad (\text{C20})$$

$$\langle \hat{p}_\mu \hat{p}_\nu \hat{p}_\zeta \rangle = 0. \quad (\text{C21})$$

The fluctuations, which diverge near $\tilde{\lambda} = 1$ (which means $\lambda = 1$), are reminiscent of what we obtain in models such as the Dicke model [9] or the Bose-Hubbard dimer [41]. There is however a key difference: In Dicke-like models, the appearance of the superradiant phase (which is associated with diverging fluctuations) coincides with the phase transition. Here, at $\lambda = 1$, the superradiant phases are still high-energy phases and the ground state is still centered around $\alpha = \beta = \gamma = 0$. The phase transition occurs only for $\lambda = 3/(2\sqrt{2})$; at this point, the semiclassical treatment we have presented predicts that the superradiant phases are already stabilized. Indeed, according to the formulas above, both the on-site fluctuations $\langle \hat{x}_i^2 \rangle$ and the cross-site correlations $\langle \hat{x}_i \hat{x}_j \rangle$ are finite for $\lambda = 3/(2\sqrt{2})$.

Note that these expressions have been obtained by a development around the solution $\alpha = \gamma = \beta = \bar{X}$. If we develop the solution around, say, $\alpha = \beta = -\gamma = -\bar{X}$, then we will obtain the Hamiltonian (C5), up to transformations $\hat{a} \rightarrow -\hat{a}$

and $\hat{b} \rightarrow -\hat{b}$. The on-site fluctuations $\langle \hat{x}_i^2 \rangle$ will remain the same, but the cross-site correlations $\langle \hat{x}_i \hat{x}_j \rangle$ will change. We will observe noise reduction for the quadratures $\hat{x}_\mu - \hat{x}_\nu$, $\hat{x}_\nu + \hat{x}_\zeta$, and $\hat{x}_\mu + \hat{x}_\zeta$. Similarly, for the other two solutions, we will find the same squeezing amount, but different squeezing directions. In the following, we will refer to the four superradiant states as $|G_{+++}\rangle$, $|G_{+--}\rangle$, $|G_{-+-}\rangle$, and $|G_{---}\rangle$.

3. Stability of the superradiant state

The analysis above allows us to make a further comment on the stability of the superradiant states. Just above $\lambda = 1$, the superradiant state can in principle exist, but quantum fluctuations can still destabilize the phase. Near the point $\lambda = 1$, we have $\langle \hat{y}^2 \rangle \sim (\tilde{\lambda} - 1)^{-1/2} \sim (\lambda - 1)^{-1/4}$, while $\langle \hat{u}^2 \rangle$ and $\langle \hat{z}^2 \rangle$ remain bounded and of order 1, because the average values $\langle \hat{u} \rangle$, $\langle \hat{y} \rangle$, and $\langle \hat{z} \rangle$ are zero everywhere. The quantum state will therefore be dominated by the fluctuations of the \hat{y} polariton and we have $\langle \hat{x}_\mu^2 \rangle \sim \langle \hat{x}_\nu^2 \rangle \sim \langle \hat{x}_\zeta^2 \rangle \sim \langle \hat{y}^2 \rangle$. We can now compare these fluctuations to the width of the well:

$$\frac{\langle \hat{x}_\mu^2 \rangle}{(X_+ - X_-)^2} \sim \frac{\langle \hat{x}_\nu^2 \rangle}{(X_+ - X_-)^2} \sim \frac{\langle \hat{x}_\zeta^2 \rangle}{(X_+ - X_-)^2} \sim \frac{U_0}{\omega\eta(\lambda - 1)^{5/4}}. \quad (\text{C22})$$

For $\lambda \lesssim 1 + l = 1 + (\frac{U_0}{\eta\omega})^{4/5}$, where $l = (\frac{U_0}{\eta\omega})^{4/5}$, the field fluctuations are of the same order of magnitude as the width of the potential well. Therefore, the quantum fluctuations can kick the system out of the local minima. Only for $\lambda \gtrsim 1 + (\frac{U_0}{\eta\omega})^{4/5}$ are the superradiant states truly well defined and (meta)stable. Alternatively, we may also compare the excitation energy with the potential barrier. The excitation energy will scale like $\omega(1 - \lambda^{1/4})$, while the potential barrier gives $E_+ - E_- \sim \frac{\omega^2\eta}{U_0}(1 - \lambda)^{3/2}$. Again, we find that the excitation energy becomes smaller than the barrier for $\lambda \gtrsim 1 + (\frac{U_0}{\eta\omega})^{4/5}$, meaning that only above this point can we suppress tunneling to the vacuum state and stabilize the superradiant state.

As of the normal phase, it will remain stable for most values of g . However, for very large values of λ , we have $E_- \rightarrow 0$; as a consequence, the potential barrier isolating the vacuum from the superradiant phase vanishes and quantum fluctuations drive the system out of the vacuum. We expect this will occur when the excitation energy in the normal phase becomes comparable to the barrier, i.e., for $\omega \sim E_-$, which gives $\lambda \sim \sqrt{\omega\eta/U_0}$ or equivalently $g_0 \sim \omega\sqrt{\eta}$. A similar order of magnitude can be obtained with the following reasoning: If we keep only the quadratic term in the Hamiltonian (1), we predict fluctuations $\langle \hat{x}_a^2 \rangle = O(1)$. Hence, the quadratic potential $\omega(\hat{a}^\dagger \hat{a} + \dots)$ will be of order ω and the trimer interaction term will be of order $\frac{g_0}{\sqrt{\eta}} \hat{x}^3 \sim \frac{g_0}{\sqrt{\eta}}$. Hence, for $g_0 \ll \sqrt{\eta}$, the interaction term will be negligible; when $g_0 \sim \sqrt{\eta}$, the interaction becomes comparable to the quadratic potential and can destabilize the normal phase. This means that this mean-field treatment predicts that the normal phase becomes unstable well after the ground state becomes superradiant.

We summarize as follows. For $\lambda < 1$, the potential has a single minimum which corresponds to the vacuum. For $1 < \lambda \lesssim 1 + (U_0/\eta\omega)^{4/5}$, four degenerate minima appear; however, the local fluctuations are still strong enough to drive the

system out of these minima. For $1 + (U_0/\eta\omega)^{4/5} \lesssim \lambda < \frac{3}{2\sqrt{2}}$, the superradiant state becomes metastable. However, its energy is still larger than the vacuum state energy. For $\lambda = \frac{3}{2\sqrt{2}}$, the superradiant and vacuum states become degenerate and a phase transition takes place. Note that at this point there is a large potential barrier between the two states, and tunneling between the vacuum and superradiant states is still suppressed: The transition is first order. For $\lambda > \frac{3}{2\sqrt{2}}$, the ground state is now superradiant; however, the vacuum remains a minimum of potential for all values of λ . For most values of λ , this minimum of potential remains deep enough to confine the field: The vacuum is still metastable. Only for $\lambda \sim \sqrt{\omega\eta/U_0}$ do the fluctuations induced by the interaction become strong enough to destabilize the vacuum. This semiclassical analysis seems to capture correctly the location of the critical point, as well as the mean number of excitations in the superradiant phase (see Fig. 1 in the main text). However, as we will shortly show, it fails to capture the divergence of the coskewness at the critical point.

4. Coskewness

a. Normal phase

We will now study the third-order moments, starting with the normal phase. As long as we remain in the vicinity of the vacuum state, the three-body coupling will only act as a perturbation. Using standard perturbation theory at first order, we find that the ground state will be given by $|000\rangle - \frac{g_0}{3\omega\sqrt{\eta}}|111\rangle$. We can immediately infer the skewness of each quadrature fluctuation:

$$\langle \hat{x}_a^3 \rangle = 0, \quad (\text{C23})$$

$$\langle \hat{x}_a^2 \hat{x}_b \rangle = 0, \quad (\text{C24})$$

$$\langle (\hat{x}_a \hat{x}_b \hat{x}_c) \rangle = \frac{-g_0}{3\omega\sqrt{\eta}}. \quad (\text{C25})$$

$$(\text{C26})$$

Equivalent expressions are obtained by permuting a , b , and c . Hence, only the three-mode phase-space distribution will be skewed. This gives

$$\mathcal{C}_{abc} = \frac{\langle \hat{x}_a \hat{x}_b \hat{x}_c \rangle}{\sqrt{\langle \hat{x}_a^2 \rangle \langle \hat{x}_b^2 \rangle \langle \hat{x}_c^2 \rangle}} \propto -\frac{g_0}{\omega\sqrt{\eta}}. \quad (\text{C27})$$

Hence, the coskewness in the normal phase is negative and tends to zero when η tends to infinity. This is indeed what we observe in Fig. 2 of the main text. Additionally, we can also derive the expression

$$\begin{aligned} \left\langle \left(\frac{\hat{x}_a + \hat{x}_b + \hat{x}_c}{\sqrt{3}} \right)^3 \right\rangle &= \left\langle \left(\frac{\hat{x}_a - \hat{x}_b - \hat{x}_c}{\sqrt{3}} \right)^3 \right\rangle \\ &= \left\langle \left(\frac{-\hat{x}_a - \hat{x}_b + \hat{x}_c}{\sqrt{3}} \right)^3 \right\rangle \\ &= \left\langle \left(\frac{-\hat{x}_a + \hat{x}_b - \hat{x}_c}{\sqrt{3}} \right)^3 \right\rangle = \frac{-g_0}{3\omega\sqrt{\eta}}. \end{aligned} \quad (\text{C28})$$

This means that the distribution of the four quadratures above is biased towards negative values. The directions towards which the distribution is biased correspond precisely to the four possible directions of displacement in the superradiant phase. This is very similar to Dicke-like transitions, in which the distribution in phase space prior to the transition is distorted along the axis of displacement in the superradiant phase. Here, however, the transition is first order, which means that we expect an abrupt transition from a skewed distribution centered around the vacuum to a fourfold-displaced distribution.

b. Superradiant phase

Let us now look at the coskewness in the superradiant phase. In the thermodynamic limit, semiclassical and Gaussian theories lead to a fourfold-degenerate ground state composed of any superposition of four displaced squeezed states. However, numerical simulations show that for physical (finite) values of η the gap decreases in the proximity of the expected critical point but is never exactly vanishing. The ground state is then well approximated by the superposition of the four superradiant states, which is in the same parity subspace of the ground state in the normal phase (the vacuum). We show in the following that this leads to accurate predictions for the value of the coskewness deep in the superradiant phase but, as expected, it cannot explain the divergence in proximity of the critical point. If we neglect quantum fluctuations and consider coherent states, the ground state would then be given by

$$\begin{aligned} |G\rangle &= \frac{1}{2}(|\bar{X}, \bar{X}, \bar{X}\rangle + |-\bar{X}, -\bar{X}, \bar{X}\rangle \\ &+ |-\bar{X}, \bar{X}, -\bar{X}\rangle + |\bar{X}, -\bar{X}, -\bar{X}\rangle). \end{aligned} \quad (\text{C29})$$

The three-body correlations are given by

$$\langle G|\hat{x}_a \hat{x}_b \hat{x}_c|G\rangle = 8\bar{X}^3.$$

The result is given by the sum of four equivalent contributions of the diagonal terms. The nondiagonal terms of the form $\langle \bar{X}, \bar{X}, \bar{X}|\hat{x}_a \hat{x}_b \hat{x}_c|-\bar{X}, -\bar{X}, \bar{X}\rangle$ all cancel (indeed, $\langle \bar{X}, \bar{X}, \bar{X}|\hat{x}_a \hat{x}_b \hat{x}_c|-\bar{X}, -\bar{X}, \bar{X}\rangle = \langle \bar{X}|\hat{x}_a|-\bar{X}\rangle \langle \bar{X}|\hat{x}_b|-\bar{X}\rangle \langle \bar{X}|\hat{x}_c|\bar{X}\rangle$ and $\langle \bar{X}|\hat{x}_a|-\bar{X}\rangle = \langle \bar{X}|\hat{a}|-\bar{X}\rangle + \langle \bar{X}|\hat{a}^\dagger|-\bar{X}\rangle = 0$).

The square of each quadrature \hat{x} will give

$$\begin{aligned} \langle G|\hat{x}_a^2|G\rangle &= \frac{1}{4}[2(\langle \bar{X}|\hat{x}_a^2|\bar{X}\rangle + \langle -\bar{X}|\hat{x}_a^2|-\bar{X}\rangle)(1 + \langle \bar{X}|\bar{X}\rangle^2) \\ &+ 8\langle \bar{X}|\hat{x}_a^2|-\bar{X}\rangle \langle \bar{X}|\bar{X}\rangle] \\ &= \frac{1}{4}[4(4\bar{X}^2 + 1) + 4(4\bar{X}^2 + 3)(\bar{X}|\bar{X}\rangle^2)], \end{aligned} \quad (\text{C30})$$

where the first and second terms are given by the sum of all diagonal and off-diagonal contributions, respectively. Finally, we find that all the linear terms $\langle G|\hat{x}_i|G\rangle$ cancel. This finally yields the expression of the coskewness

$$\mathcal{C}_{abc} = \frac{8\bar{X}^3}{[4\bar{X}^2 + 1 + (4\bar{X}^2 + 3)e^{-4\bar{X}^2}]^{3/2}}. \quad (\text{C31})$$

Deep into the symmetry-broken phase, we recover $\lim_{\eta \rightarrow \infty} \mathcal{C}_{abc} = -1$ as found numerically. However, this treatment also predicts that we always have $\mathcal{C}_{abc} > -1$. Therefore, even by taking into account the superposition of

four coherent states, the semiclassical analysis cannot account for the divergence of the coskewness at the critical point.

So far we have focused on the semiclassical theory. Let us now show that including Gaussian fluctuations cannot affect significantly the value of \mathcal{C}_{abc} . For instance, let us consider the term $\langle G_{+++} | \hat{x}_a \hat{x}_b \hat{x}_c | G_{+++} \rangle$, which appears in the expression of \mathcal{C}_{abc} . We can decompose it as

$$\begin{aligned} & \langle G_{+++} | \hat{x}_a \hat{x}_b \hat{x}_c | G_{+++} \rangle \\ &= 8\bar{X}^3 + 12\bar{X}^2 \langle \hat{x}_\mu \rangle + 6\bar{X} \langle \hat{x}_\mu \hat{x}_\nu \rangle + \langle \hat{x}_\mu \hat{x}_\nu \hat{x}_\zeta \rangle \\ &= 8\bar{X}^3 + 2\bar{X} \left(\frac{1 + f_+^2}{1 + 3f_+^2} \right)^{1/2} (\langle \hat{y}^2 \rangle - \langle \hat{z}^2 \rangle). \end{aligned}$$

For $\lambda \geq \frac{3}{2\sqrt{2}}$, the second term is bounded and of order 1, including at the critical point. Therefore, since $\bar{X} \gg 1$, we

can write $\langle G_{+++} | \hat{x}_a \hat{x}_b \hat{x}_c | G_{+++} \rangle = 8\bar{X}^3 + O(\bar{X})$; the dominant term in the expression will be the same as in the absence of quantum fluctuations. The same is true for all of the terms appearing in \mathcal{C}_{abc} ; the correction due to the quantum fluctuation will always be subdominant. In the end, we will get

$$\mathcal{C}_{abc} = \frac{8\bar{X}^3 + O(\bar{X})}{8|\bar{X}|^3 + O(\bar{X}^2)} \sim -1.$$

Therefore, the superposition of four displaced squeezed states cannot account for the divergence of the coskewness at the critical point, as the quantum fluctuations predicted by the Gaussian analysis are bounded. This shows that in proximity to the critical point the system develops genuine non-Gaussian features.

-
- [1] S. Haroche, *Rev. Mod. Phys.* **85**, 1083 (2013).
- [2] G. L. Paravicini-Bagliani, F. Appugliese, E. Richter, F. Valmorra, J. Keller, M. Beck, N. Bartolo, C. Rössler, T. Ihn, K. Ensslin, *et al.*, *Nat. Phys.* **15**, 186 (2019).
- [3] E. Cortese, N.-L. Tran, J.-M. Manceau, A. Bousseksou, I. Carusotto, G. Biasiol, R. Colombelli, and S. De Liberato, *Nat. Phys.* **17**, 31 (2021).
- [4] F. Herrera and J. Owrutsky, *J. Chem. Phys.* **152**, 100902 (2020).
- [5] J. Fregoni, F. J. Garcia-Vidal, and J. Feist, *ACS Photon.* **9**, 1096 (2021).
- [6] P. Forn-Díaz, L. Lamata, E. Rico, J. Kono, and E. Solano, *Rev. Mod. Phys.* **91**, 025005 (2019).
- [7] A. Frisk Kockum, A. Miranowicz, S. De Liberato, S. Savasta, and F. Nori, *Nat. Rev. Phys.* **1**, 19 (2019).
- [8] A. Le Boité, *Adv. Quantum Technol.* **3**, 1900140 (2020).
- [9] P. Kirton, M. M. Roses, J. Keeling, and E. G. Dalla Torre, *Adv. Quantum Technol.* **2**, 1800043 (2019).
- [10] D. De Bernardis, P. Pilar, T. Jaako, S. De Liberato, and P. Rabl, *Phys. Rev. A* **98**, 053819 (2018).
- [11] A. Stokes and A. Nazir, *Nat. Commun.* **10**, 499 (2019).
- [12] O. Di Stefano, A. Settineri, V. Macrì, L. Garziano, R. Stassi, S. Savasta, and F. Nori, *Nat. Phys.* **15**, 803 (2019).
- [13] G. M. Andolina, F. M. D. Pellegrino, V. Giovannetti, A. H. MacDonald, and M. Polini, *Phys. Rev. B* **100**, 121109(R) (2019).
- [14] P. Nataf and C. Ciuti, *Nat. Commun.* **1**, 72 (2010).
- [15] J. J. Garcia-Ripoll, B. Peropadre, and S. De Liberato, *Sci. Rep.* **5**, 16055 (2015).
- [16] V. E. Manucharyan, A. Baksic, and C. Ciuti, *J. Phys. A: Math. Theor.* **50**, 294001 (2017).
- [17] D. De Bernardis, T. Jaako, and P. Rabl, *Phys. Rev. A* **97**, 043820 (2018).
- [18] I. M. Georgescu, S. Ashhab, and F. Nori, *Rev. Mod. Phys.* **86**, 153 (2014).
- [19] N. K. Langford, R. Sagastizabal, M. Kounalakis, C. Dickel, A. Bruno, F. Luthi, D. J. Thoen, A. Endo, and L. DiCarlo, *Nat. Commun.* **8**, 1715 (2017).
- [20] J. Braumüller, M. Marthaler, A. Schneider, A. Stehli, H. Rotzinger, M. Weides, and A. V. Ustinov, *Nat. Commun.* **8**, 779 (2017).
- [21] D. Marković, S. Jezouin, Q. Ficheux, S. Fedortchenko, S. Felicetti, T. Coudreau, P. Milman, Z. Leghtas, and B. Huard, *Phys. Rev. Lett.* **121**, 040505 (2018).
- [22] D. Lv, S. An, Z. Liu, J.-N. Zhang, J. S. Pedernales, L. Lamata, E. Solano, and K. Kim, *Phys. Rev. X* **8**, 021027 (2018).
- [23] G. A. Peterson, S. Kotler, F. Lecocq, K. Cicak, X. Y. Jin, R. W. Simmonds, J. Aumentado, and J. D. Teufel, *Phys. Rev. Lett.* **123**, 247701 (2019).
- [24] A. Dareau, Y. Meng, P. Schneeweiss, and A. Rauschenbeutel, *Phys. Rev. Lett.* **121**, 253603 (2018).
- [25] F. Mivehvar, F. Piazza, T. Donner, and H. Ritsch, *Adv. Phys.* **70**, 1 (2021).
- [26] A. T. Black, H. W. Chan, and V. Vuletić, *Phys. Rev. Lett.* **91**, 203001 (2003).
- [27] K. Baumann, C. Guerlin, F. Brennecke, and T. Esslinger, *Nature (London)* **464**, 1301 (2010).
- [28] Z. Zhiqiang, C. H. Lee, R. Kumar, K. Arnold, S. J. Masson, A. Parkins, and M. Barrett, *Optica* **4**, 424 (2017).
- [29] S. Ashhab, *Phys. Rev. A* **87**, 013826 (2013).
- [30] M.-J. Hwang, R. Puebla, and M. B. Plenio, *Phys. Rev. Lett.* **115**, 180404 (2015).
- [31] M. Liu, S. Chesi, Z.-J. Ying, X. Chen, H.-G. Luo, and H.-Q. Lin, *Phys. Rev. Lett.* **119**, 220601 (2017).
- [32] M.-J. Hwang, P. Rabl, and M. B. Plenio, *Phys. Rev. A* **97**, 013825 (2018).
- [33] R. Puebla, M.-J. Hwang, J. Casanova, and M. B. Plenio, *Phys. Rev. Lett.* **118**, 073001 (2017).
- [34] J. Larson and E. K. Irish, *J. Phys. A: Math. Theor.* **50**, 174002 (2017).
- [35] J. Peng, E. Rico, J. Zhong, E. Solano, and I. L. Egusquiza, *Phys. Rev. A* **100**, 063820 (2019).
- [36] L. Innocenti, G. D. Chiara, M. Paternostro, and R. Puebla, *New J. Phys.* **22**, 093050 (2020).
- [37] Z.-J. Ying, *Adv. Quantum Technol.* **5**, 2100088 (2022).
- [38] J. Zhao and M.-J. Hwang, *Phys. Rev. Lett.* **128**, 163601 (2022).
- [39] R. Palacino and J. Keeling, *Phys. Rev. Res.* **3**, L032016 (2021).
- [40] A. Baksic and C. Ciuti, *Phys. Rev. Lett.* **112**, 173601 (2014).
- [41] S. Felicetti and A. Le Boité, *Phys. Rev. Lett.* **124**, 040404 (2020).

- [42] L. Garbe, M. Bina, A. Keller, M. G. A. Paris, and S. Felicetti, *Phys. Rev. Lett.* **124**, 120504 (2020).
- [43] P. A. Ivanov, *Phys. Rev. A* **102**, 052611 (2020).
- [44] S. Wald, S. V. Moreira, and F. L. Semião, *Phys. Rev. E* **101**, 052107 (2020).
- [45] K. Gietka, F. Metz, T. Keller, and J. Li, *Quantum* **5**, 489 (2021).
- [46] Y. Chu, S. Zhang, B. Yu, and J. Cai, *Phys. Rev. Lett.* **126**, 010502 (2021).
- [47] R. Di Candia, F. Minganti, K. Petrovnin, G. Paraoanu, and S. Felicetti, [arXiv:2107.04503](https://arxiv.org/abs/2107.04503).
- [48] M. Salado-Mejía, R. Román-Ancheyta, F. Soto-Eguibar, and H. M. Moya-Cessa, *Quantum Sci. Technol.* **6**, 025010 (2021).
- [49] L. Garbe, O. Abah, S. Felicetti, and R. Puebla, *Quantum Sci. Technol.* **7**, 035010 (2022).
- [50] K. Gietka, L. Ruks, and T. Busch, *Quantum* **6**, 700 (2022).
- [51] L. Garbe, O. Abah, S. Felicetti, and R. Puebla, *Phys. Rev. Res.* **4**, 043061 (2022).
- [52] K. Gietka, *Phys. Rev. A* **105**, 042620 (2022).
- [53] T. Ilias, D. Yang, S. F. Huelga, and M. B. Plenio, *PRX Quantum* **3**, 010354 (2022).
- [54] C. W. S. Chang, C. Sabín, P. Forn-Díaz, F. Quijandría, A. M. Vadiraj, I. Nsanzineza, G. Johansson, and C. M. Wilson, *Phys. Rev. X* **10**, 011011 (2020).
- [55] I. Carusotto and C. Ciuti, *Rev. Mod. Phys.* **85**, 299 (2013).
- [56] K. Binder and D. P. Landau, *Phys. Rev. B* **30**, 1477 (1984).
- [57] X. Gu, A. F. Kockum, A. Miranowicz, Y. xi Liu, and F. Nori, *Phys. Rep.* **718–719**, 1 (2017).
- [58] A. Blais, A. L. Grimsmo, S. M. Girvin, and A. Wallraff, *Rev. Mod. Phys.* **93**, 025005 (2021).
- [59] S. Fedortchenko, S. Felicetti, D. Marković, S. Jezouin, A. Keller, T. Coudreau, B. Huard, and P. Milman, *Phys. Rev. A* **95**, 042313 (2017).
- [60] A. Agustí, C. W. S. Chang, F. Quijandría, G. Johansson, C. M. Wilson, and C. Sabín, *Phys. Rev. Lett.* **125**, 020502 (2020).
- [61] A. A. Casado and C. Sabín, *Phys. Rev. A* **105**, 022401 (2022).
- [62] H. Breuer and F. Petruccione, *The Theory of Open Quantum Systems* (Oxford University Press, Oxford, 2007).
- [63] E. M. Kessler, *Phys. Rev. A* **86**, 012126 (2012).
- [64] F. Minganti, A. Biella, N. Bartolo, and C. Ciuti, *Phys. Rev. A* **98**, 042118 (2018).
- [65] H. J. Carmichael, *Statistical Methods in Quantum Optics 2* (Springer, Berlin, 2008).
- [66] B. Baumgartner and N. Heide, *J. Phys. A: Math. Theor.* **41**, 395303 (2008).
- [67] B. Buča and T. Prosen, *New J. Phys.* **14**, 073007 (2012).
- [68] V. V. Albert and L. Jiang, *Phys. Rev. A* **89**, 022118 (2014).
- [69] R. Puebla, *Phys. Rev. B* **102**, 220302(R) (2020).
- [70] M. G. Genoni, M. G. A. Paris, and K. Banaszek, *Phys. Rev. A* **76**, 042327 (2007).
- [71] M. G. Genoni, M. G. A. Paris, and K. Banaszek, *Phys. Rev. A* **78**, 060303(R) (2008).
- [72] R. Filip and L. Mišta, *Phys. Rev. Lett.* **106**, 200401 (2011).
- [73] M. Walschaers, *PRX Quantum* **2**, 030204 (2021).
- [74] S. Lieu, R. Belyansky, J. T. Young, R. Lundgren, V. V. Albert, and A. V. Gorshkov, *Phys. Rev. Lett.* **125**, 240405 (2020).